Journal of the European Ceramic Society 20 (2000) 607–618

Processing and properties of an all-oxide composite with a porous matrix

J.J. Haslam, K.E. Berroth*, F.F. Lange

Materials Department, University of California at Santa Barbara, Santa Barbara, CA 93106, USA

Accepted 18 August 1999

Abstract

Processing and mechanical properties of an all-oxide fiber composite with a porous matrix are presented here. The processing approach for an all-oxide composite was developed to be simple and involve one sintering process. The composite uses a porous matrix instead of riser coatings to deflect cracks from the fibers. A processing method involving recently developed methods for reshaping and forming saturated high-volume fraction (> 50 vol%) particle bodies was used to form the composite. Good infiltration of the woven fiber tows was obtained. Sintering in a pure HCl gas atmosphere was used to produce a porous matrix without shrinkage during processing. The sintering process also produced coarsening which makes the microstructure stable against densification during use and thereby prevents forming cracklike voids and retains sufficient porosity for crack deflection. Measurements of interlaminar shear strength and strength of the composite show that composite produced by this processing method is comparable to previous all-oxide materials produced using the oxide fibers used here. The mechanical properties are rationalized in terms of the features on the fracture surfaces. Disintegration of the matrix to allow energy dissipation during fracture was apparent and correlates with the measurements of the fracture toughness of the material. Moderate notch insensitivity was demonstrated with a net section strength in the presence of a notch being 700% of the unnotched strength.

Keywords: Aluminosilicate fibres; Composites; Mechanical properties; Porosity; Sintering; ZrO_2 matrix

1. Introduction

An important property of any ceramic matrix composite (CMC) is that its strength should be relatively insensitive to the presence of notches. If the riders within a CMC are effective, the strength of a body with a notch (or hole) of any size or shape will be the same as the unnotched strength of a body with same net (or reduced) cross-section. That is, for an ideal CMC, one should be able to drill a hole without significantly reducing the failure load other than the effect of reducing its cross sectional area.

Since the failure strain of a strong fiber is generally much larger than a dense matrix, cracks generally first extend within the matrix. In terms of crack extension, notch insensitivity requires that the fibers must be isolated from the very high stress field of a crack within the matrix. A fiber within a good CMC is only expected to break when the applied load exceeds its strength.

In the late 1960s Phillips[1] recognized that brittle, but strong fibers could be isolated from one another within a brittle matrix by providing a path for cracks propagating through the matrix to bypass the fibers. A 'weak' interface between the matrix and fiber provides the path for crack deflection, thus allowing the crack to propagate along the fiber/matrix interface instead of through the fiber. As described by He and Huchinson,[2] the condition for crack deflection depends on the ratio of the critical strain energy release rate for the interface and fiber, and the elastic properties of the two materials. For a few fiber/matrix combinations, the crack defecting interface needs no special processing conditions. For example. the carbon fibers in the CMCs produced by Phillips et al. did not bond to the glass matrix. For most other CMCs, the fibers must be coated with either carbon or boron nitride films to achieve a crack deflecting interface. Not only do fiber coatings introduce cost and processing complexity, but they are not stable in oxidizing environments and they can cause composite embrittlement.

* Corresponding author. Visiting Researcher, High Performance Ceramic Section, Swiss Federal Laboratories for Materials Testing and Research, EMPA, Dübendorf, Switzerland.

0955-2219/00/$ - see front matter
PII: S0955-2219(99)00259-9

Cracking phenomena for the tensile loading of a unidirectional CMC containing crack deflecting interfaces can be related to the composite's stress/strain behavior. During the initial loading, the behavior is linear and characterized by the combined elastic modulus of the fiber and matrix weighted by the appropriate volume fraction of each. As loading proceeds, matrix cracking initiates without fiber failure. Matrix cracking is characterized by a decreased slope of the stress–strain curve. Multiple matrix cracking generally occurs prior to the initiation of fiber failure. Prior to and during fiber failure, the cracked matrix is held together by the fibers, which now supports nearly all of the applied load. Fiber failure, and thus CMC failure occurs at a high strain (0.5 to 1.0%), indicative of a strong fiber with a low elastic modulus. For many commercial and experimental CMCs the stress for matrix cracking lies between 40 and 100 MPa whereas composite failure (fiber failure) does not occur until the stresses exceed 150 to 300 MPa. Thus, CMCs that have been developed over the last 25 years to contain crack deflecting interfaces can not only be relatively notch insensitive, but they can also exhibit higher strains to failure relative to monolithic ceramics (e.g. Si_3N_4, with a mean tensile strength of 1000 MPa, has a strain to failure of 0.3%).

Approximately 5 years ago another type of CMC was inadvertently discovered.[3,4] Unlike the CMCs with 'weak' fiber matrix interfaces, the matrix and fibers are bonded together in these 'new' CMCs. The second change is that the matrix in the 'new' CMCs is purposely made to be porous. Despite these two major changes, both of which are not taught by mechanics of conventional CMCs, the new CMC with well-bonded fiber/matrix interfaces and porous matrixes are notch insensitive. In addition, although not as high as the conventional CMCs, their failure strain is larger than conventional monolithic ceramics.[5]

The mode of failure of these new composites is different from the older CMCs.[4] The stress/strain behavior of tensile specimens is nearly linear to failure, indicating that both the matrix and fibers fail at about the same failure strain.[5] Tensile failure can occur at ≈200 MPa; the strength is also relatively notch insensitive.[5] These new CMCs can be processed with oxide fibers in an oxide matrix and can be very stable in air to temperatures where the fibers begin to degrade. It can be expected that the processing of the new CMCs is much less complex and less costly. Eliminating fiber coatings is a significant advantage in processing and reducing cost.

The porous matrix appears to play a critical role in achieving a notch insensitive strength and a high failure strain. One role concerns the strain to failure. When a composite is loaded in tension, the fibers will support much of the load due to their much larger elastic modulus relative to the porous matrix. Although the fiber must carry the major portion of the stress, the strain within the fibers and matrix is identical. It is possible that the failure strain (ε_m) of the porous matrix can be equal or even larger than the failure strain of the fibers (ε_f). Applying Hook's Law, one can show that

$$\varepsilon_f = \varepsilon_m, \text{ or } \frac{\sigma_f}{E_f} = \frac{\sigma_m}{\varepsilon_m}, \quad (1)$$

where $\varepsilon_{m,f}$ and $E_{m,f}$ are the failure stress and elastic modulus of the matrix (m) and fibers (f). Using properties of a low density Al_2O_3 matrix material and Al_2O_3 fibers (e.g. $\sigma_m \approx 200$ MPa, $\sigma_f \approx 2000$ MPa, $E_m \approx 40$ GPa and $E_f = 400$ GPa) we can see that it is reasonable to be able to fabricate a porous matrix with a failure strain that approaches that of a strong fiber. Therefore, in tension, a large fraction of the strength and strain to failure of strong fibers can be achieved in a ceramic composite that contains a porous matrix.

The second role of the porous matrix is to allow fibers to be isolated from cracks within the matrix. In porous materials the crack front can be non-continuous and crack extension must occur by the continued breaking of the solid phase units, i.e. fracture has to be reinitiated in the solid phase within the high stress field of the propagating crack. A comparable example of this fracture mode is the extension of a crack within cloth, where the fracture of each fiber is independent of the last to fail. This mode of crack extension occurs in powder compacts that have been heated to produce necks between touching particles. Observing the fracture surface of these very porous materials one can see that fracture (or 'crack extension') occurred by the breaking of grain pairs at grain boundaries.[6] A continuous crack front does not exist in these porous materials.

The lack of a crack front in a porous matrix means that embedded fibers never see an extending crack front as the matrix fails. Fiber fracture within a very porous matrix must initiate within the fiber itself. i.e. from flaws either on the surface or within the fiber, and not by the propagation of a crack within the matrix. Thus, fibers in a very porous matrix can fracture in the same manner as they do when they exist as a bundle, without a matrix. The high failure strain of the fibers becomes the failure strain of the composite because the matrix will have a comparable strain to failure.

As detailed elsewhere,[3–5] one method to produce the fiber composites described above is to pack particles around the fibers within a fiber preform by pressure filtration and then strengthen the porous matrix. In this method, a fiber preform (3-D weave, stacked layers of cloth, etc.) is mounted on a filter within a die cavity. A pressure is exerted to a dispersed slurry to cause the particles to stream though the preform to become trapped at the filter, and to build up a consolidated layer within the fiber preform. The slurry must be formulated such that the particles are repulsive with respect to themselves and the fibers. The particles must also be

much smaller than the fiber diameter to ensure good particle packing.[7] To avoid large, cracklike voids from developing within the matrix, the powder should not densify during subsequent heat treatments and at application temperatures.[8,9] For this reason, in our previous work we used a mullite powder that did not begin to shrink until ≈1300°C, the maximum fiber application temperature. After removing the liquid via evaporation, the powder matrix was strengthened by infiltrating the composite with a solution containing precursor molecules. After evaporating the liquid, heating causes the precursor molecules to decompose to form an inorganic material that bonds the particles together. The inorganic phase that bonds and strengthens the powder matrix also bonds the particles (matrix) to the fibers. Cyclic solution precursor infiltration, evaporation, and decomposition further strengthens the matrix phase. Care must be taken to avoid precursor molecules from migrating to the surface during evaporation. This condition produces surface cracking during drying due to a thin layer of precursor molecules that form on the surface.[10] An all-oxide, fiber reinforced ceramic composite can be processed in this method. Extensive mechanical testing by Levi et al.[5] has shown that this type of composite can exhibit a significant notch insensitive strength in tensile loading. It also has all the attributes found for fiber reinforced ceramics fabricated with dense matrixes and weak fiber/matrix interfaces.

Here we report a much simpler and less time consuming fabrication method for processing these new CMCs with porous matrices. In the new method, the powder is treated to produce a special interparticle pair potential which allows the powder compact (previously consolidated by pressure filtration) to be fluidized. It can then be formed into a thin sheet by vibrating between plastic sheets. The plastic sheets help to avoid evaporation and the consequent drying of the thin particle layers. The ceramic sheet is then frozen to enable removal from between the plastic sheets. The frozen ceramic sheet of powder is then sandwiched between sheets of ceramic fibers (e.g. woven cloth). After thawing, the powder sheet is fluidized by vibrating. It then flows to surround all fibers in the adjacent fiber sheets After evaporation, the powder surrounding the fibers can be made strong either by the use of precursors described above or by an HCl evaporation/condensation treatment described below. Preliminary mechanical measurements show that this new route can result in similar properties as the previous route to manufacture CMCs with porous matrices.

2. Experimental

2.1. Composite processing

Composites were formed from layers of two dimensional, 8 harness woven cloth of Nextel™ 720 fiber tows produced by the 3M Corporation (St. Paul, MN). Each tow nominally contains 420 fibers. The Nextel 720 fiber is an experimental fiber composed of a mixture of submicron alumina and mullite grains. The two interpenetrating phases ensure a small grain size during processing. The mullite in the fiber contributes to high creep resistance compared to a similar all-alumina fiber (Nextel 610). The strength of the Nextel 720 fiber is about 30% less than the 610 for single filament properties,[11] but it was selected because of its greater creep resistance.[12]

As detailed below, laminated ceramic cloth was infiltrated with a previously consolidated mixture of 70 vol% cubic zirconia (solid solution with 8 mol% Y_2O_3, TZ8YS, Toso Ceramics, average particle diameter of (0.4 μm) and 30 vol% mullite (MU-107, Showa Denko). As detailed below and elsewhere, zirconia was used as the matrix because it can be sintered, without shrinkage, when heat treated in HCl at temperatures as low as 1100°C.[13] Mullite was introduced because previous work has shown that mullite does not allow the sintered and coarsened zirconia to shrink (densify) after exposure to air at 1200°C for 100 h.[6] The zirconia was composed of agglomerated particles which contained primary particles of 50–100 nm in diameter. Infrared spectroscopy indicated that the mullite contained an organic contaminant that had to be removed from the powder before it was formulated as a slurry. A 10 h heat treatment in air at 800°C was sufficient to remove the contaminant. The particle size (average = 0.7μm) did not change during the heat treatment.

Dispersed, aqueous slurries containing 20 vol% of the two powders were formed by adding 1.3 vol% polyethylene oxide urethane silane (PEG-silane, Gelest, Inc.) at pH 10.5. This was found to be sufficient to coat the particle surfaces. As detailed elsewhere, the PEG-silane molecules chem-adsorb to the particles by reacting with the -M–OH (M = metal atom) surface sites.[14,15] The zirconia slurry was attrition milled for 15 min after the powder was added. The mullite slurry was sonnicated with an ultrasonic horn for 5 min prior to the final adjustment of the pH. Tetraethylammonium chloride TEACl) salt (0.1 molar) was added to form weakly attractive pair potentials between the particles. As detailed elsewhere, TMA^+ counter ions aid in producing a weakly attractive particle network which can be packed to a high density via pressure filtration and allow the consolidated body to be fluidized via vibration.[16–18] TEA^+ counter ions were used in this work; these counter ions are slightly larger than TMA^+. Other methods can be used to produce weakly attractive networks such as surfactants or chemi-sorption of alcohols.[19] The PEG-silane plus TEACI approach was appropriate here due to the two different powders used to form a composite slurry The two slurries were mixed in appropriate portions described above. The mixed

slurry was then consolidated by pressure filtration at 5 MPa to form disc shaped bodies that were fully saturated with water. The saturated bodies were stored in sealed plastic bags containing a small paper towel saturated with water to help prevent drying. The volume fraction of powder within the saturated, consolidated bodies was determined by weight difference method as 52%.[15] At a later time, the consolidated powder compact (or a portion cut with a razor blade) was placed between two plastic sheets (e.g. a bag) and fluidized with an air-powered vibrator into uniform ~300 μm thick 'tapes' of consolidated particles.

An illustration of the composite processing steps is shown in Fig. 1. Initially, tapes are formed by pressing the fluidized sheets in between two flat steel plates using two spacer bars to fix the thickness. The pressed tapes were flexible due to the weakly attractive particle potential. The tapes, still between the plastic sheets, were frozen to facilitate composite processing and/or storage.

To produce the composite, the frozen tapes were removed from between the plastic sheets and sandwiched between two layers of woven, fiber cloth. Sandwiches with up to 27 layers, (14 weaves and 13 frozen ceramic tapes) were piled up, packed in plastic, evacuated, and sealed in plastic. After thawing, the assembled layers were vibrated and pressed lightly in between two steel plates with appropriate spacers to cause the fluidized powder to flow and intrude the finer layers. Multi-layer composites in sizes of $40\times100\times3$ mm could be fabricated by this vibration supported single step impregnation. The multi-layer cloth composite could then be dried or frozen for later use. It should be noted that the layers of fiber cloth, impregnated with the fluidized powder ceramic compact as described were very flexible and could be shaped much like a sheet of uncross-linked carbon fiber/epoxy prepreg.

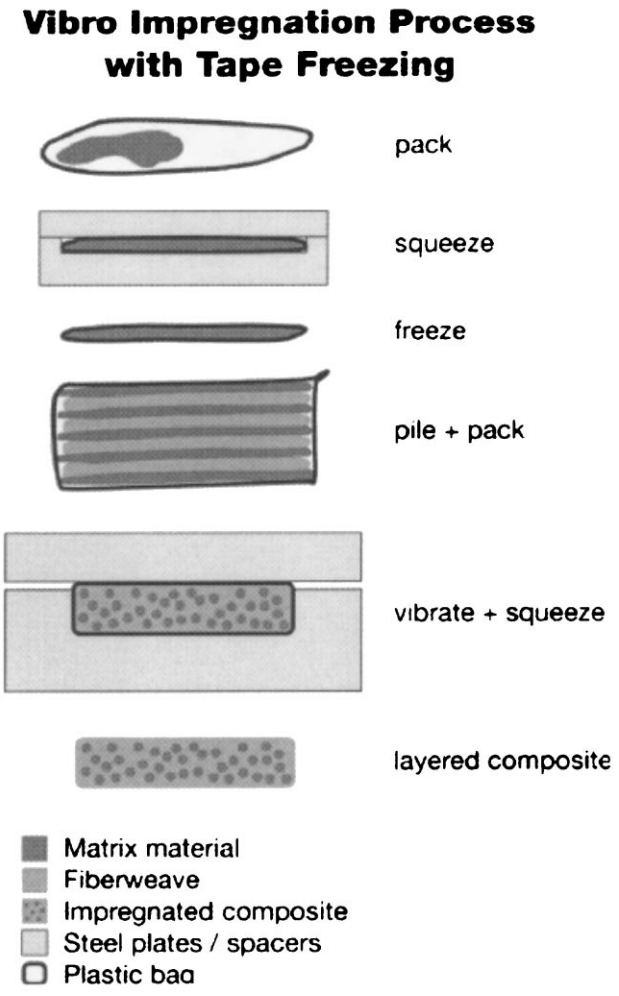

Fig. 1. This illustration shows the processing steps used to form the composite.

Further processing requires removing the water from the saturated powder matrix by drying in an oven at ≈70°C, and then sintering the ZrO_2 in a dry HCl gas environment at temperatures between 1200 and 1300°C.[20] As reported elsewhere[21] the HCI gas heat treatment did not affect the strength of fiber bundles. With the knowledge of the volume of fibers per unit area of cloth, the volume fraction of floors within the composite was determined by measuring the volume of the composite and counting the number of fiber layers in each specimen. For composites fabricated for this study, the average volume fraction of fibers was 0.37 ± 0.02.

2.2. Interlaminar shear tests

For some design considerations, a desirable property of a woven, layered composite is to have sufficient interlaminar shear strength to resist delamination. This type of failure might be encountered in a bending type of loading through the thickness as encountered with a through-thickness temperature gradient. Interlaminar shear strength was determined with 0°/90° bar specimens ($3.5\times7\times20$ mm nominal dimensions) diamond cut from larger plates fabricated with 12 or more cloth layers. The specimen edges were diamond ground (400 grit) to remove a minimum 300 μm of damage introduced by the diamond cutting. 3-Point flexural tests were performed where the span was changed for reasons discussed below. The fiber weave orientation was horizontal with the loading in the vertical direction as shown in Fig. 2(a). Nylon rods (6.45 mm diameter) were

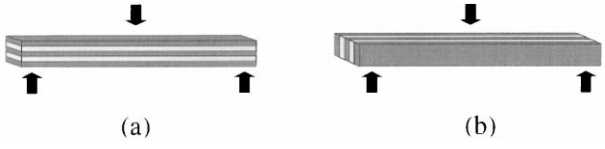

Fig. 2. Schematic of fiber orientation of composite for bending tests. (a) Interlaminar Shear Strength tests. (b) In-plane bend testing for flexural strength and elastic modulus.

used as loading pins to accommodate the inherent roughness of the woven fibers on the specimen surface and to reduce contact loading stress. No permanent deformation of the loading rods was observed after testing, which indicates that they remained elastic under the stresses encountered in testing. A servo-electric testing machine (Instron, Inc. model 8562) with a high stiffness frame was used to load the specimens at a cross head speed of 0.1 mm/min.

The shear stress at the mid-plane of a flexural bar specimen can be calculated from beam theory as:

$$\tau = 3/4^{*}L/(W^{*}t), \tag{2}$$

where L = load, w = width, and t = thickness. The measurement of delamination stress for CMCs usually prescribes a span (S) to thickness ratio (S/t) of greater than 10 to help insure that the specimen fails by delamination (shear) rather than a tensile failure on the surface, given by

$$\sigma = \frac{3/2^{*}P^{*}S}{(b^{*}t^{2})}. \tag{3}$$

The midplane shear stress to maximum tensile stress ratio (τ/σ) is given by

$$\tau/\sigma = 1/2(t/S). \tag{4}$$

Therefore, for a given specimen thickness, the shorter the span, the greater the probability that failure will take place by a delamination of the cloth layers, rather than crack extension through the layers. Flexural testing with small values of S/t is called short beam bend testing and is used to characterize the interlaminar shear strength.

2.3. In-plane flexure testing of notched and un-notched specimens

Attempts to perform tensile tests on 100 mm long specimens (same material as above) with a reduced gauge section (5.1 mm wide, 40 mm long, produced with a 152 mm diameter diamond grinding wheel) were not successful with our limited amount of material. Despite the use of fiberglass tabs that were epoxied to the ends of the specimen and double knife-edge universal joints within the tensile train, most specimens failed either in the non-reduced gauge section or adjacent to the clamping grip.

Because of the limited amount of fiber cloth available for fabricating specimens, the implementation of an improved tensile test was not possible. The testing mode was changed to an in-plane flexural test, subjected to 3-point flexural loading as shown in Fig. 2(b). This configuration and loading mode allowed for testing of the composite strength in bending without interlaminar shear type failures. Strain was calculated based on measurements of the bottom beam displacement. In addition, based on a technique used by Heathcote et al.,[22] notched bending tests were performed in a similar manner. Two different bar specimens ($3.5\times7\times90$ mm and $3.5\times7\times45$ mm nominal dimensions) were tested in 3-point flexural load with an outer span of 35 mm and 89 mm for the shorter and longer specimens respectively. The cross head displacement rate was 0.1 mm/min. Two different fiber alignments were tested, one with $0^{\circ}/90^{\circ}$ and one with $+/-45^{\circ}$ fiber directions relative to the direction of the bar length.

Notches were cut in the center of bars with a diamond wheel with a resulting notch thickness of 0.55 mm. The notch depth was nominally one half of the sample height, $a/W = 0.485 \pm 0.015$. The high stiffness of the testing machine/load cell, and the non-catastrophic failure of the specimens allowed for careful measurement of the energy required to break the notched specimens. The measured projected surface area of the sample was used to calculate energy per unit area to produce fracture.

The stress–strain response of the un-notched composites was nearly linear elastic with some significant deviations in the $+/-45^{\circ}$ fiber direction tests. Due to the low loads encountered in testing specimens of this length, no damage was observed at the loading points. The specimens were tested in the same high-stiffness universal testing machine used for the interlaminar shear strength tests.

3. Results

3.1. Interlaminar shear strength

Fig. 3 reports the apparent interlaminar shear strength as a function of span to thickness ratio (S/t) for individual CMC specimens heat treated in HCI for different time periods and temperatures. As shown, the delamination stress was $\approx 10 \pm 2$ MPa for all heat treatments, and that specimens produced from one heat treatment (1250°C/5 h) failed in tension and did not delaminate. Fig. 3 also reports the delamination stress reported by Levi et al.[5] for a CMC with a porous matrix, but fabricated by the older method (pressure filtration, multiple precursor infiltration and pyrolysis cycles). Its delamination strength of 8 MPa is a little lower than most of the values reported for our newer method but Levi et al. used harder, steel loading pins, which could have produced a stress concentration and a lower delamination stress.[5]

Figs. 4 and 5 illustrate typical stress versus strain plot for specimens that delaminated prior to tensile failure. In general, one or two load drops were observed similar

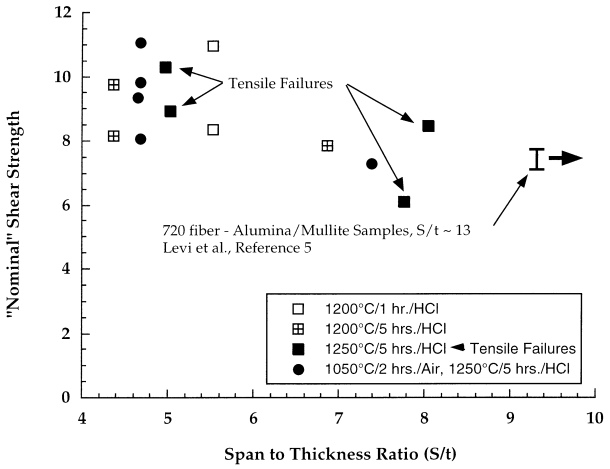

Fig. 3. Plot of 'nominal' interlaminar shear strength against span to thickness ratio for a variety of samples. The 1250°C/5 h/HCl samples failed in a tensile failure mode which implies that the interlaminar shear strength is greater than these values.

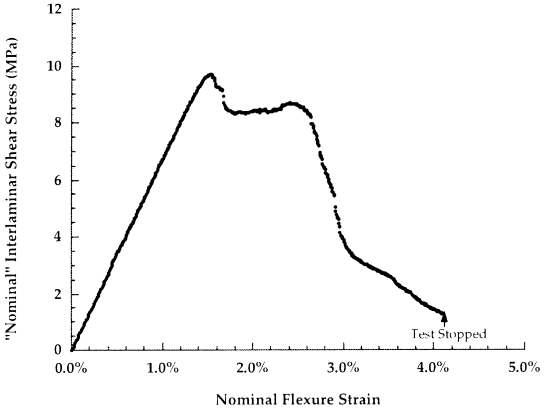

Fig. 4. 'Nominal' Interlaminar shear strength test result: 0/90° fiber orientation sintered in HCl at 1200°C, 5s.

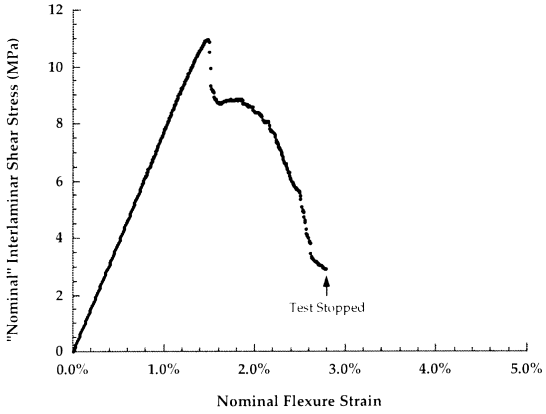

Fig. 5. 'Nominal' Interlaminar shear strength test result: 0/90° fiber orientation sintered in HCl at 1250°C, 5h.

to the phenomenon of sequential, delamination failure.[23] A slight reduction in stiffness was observed near the peak loads. At the first load drop, cracking was usually not evident under low magnification (2–3X), but the cracks became apparent after loading beyond the initial load drop.

3.2. In-plane flexure testing

Table 1 reports the in-plane mechanical properties for un-notched 0°/90° and +/−45° oriented composite specimens processed in HCI for different conditions. The strength of the 0°/90° specimens was >160 MPa, and the strength of the +/−45° specimens was >80 MPa consistent with those reported by Levi et al.[5] for the previous method of processing the porous matrix composites. Fig. 6 shows representative stress–strain curves for 0°/90° and +/−45° composites (1250°C/5h/HCl); their respective failure strains were 0.25 and 0.2%.

Table 2 reports the in-plane mechanical properties of the notched specimens 0°/90° and +/−45° oriented composite specimens processed with the same conditions as the un-notched specimens (Table 1). Strength values are reported for a 'net cross-sectional area' specimen, i.e. assuming that the bar dimensions used to calculate the maximum tensile stress at failure [Eq. (2)] does not include the notched portion of the bar. As shown, the strength of the notched bars, based on the 'net cross-sectional area' is ≈70% of the un-notched bars, regardless of fiber orientation. Fig. 7 shows the load/displacement curves for representative 0°/90° and +/−45° notched specimens. It can be seen that the failure was not catastrophic, and the work of fracture, reported in Table 2, could be determined by measurements of the area under the curve. The work of fracture for the 0°/90° specimens was 3–4 times greater than the +/−45° oriented specimens. Fig. 8, a photograph of one of the fractured, notched 0°/90° oriented specimen, illustrates that interlocking fibers still hold the bar together after the applied load is removed. It was observed that both notched and un-notched specimens did not fall apart after the load was removed.

Table 1
Properties of in-plane un-notched composite 3-point bend tests

Fiber	Sintering	Flexure Strength MPa	Elastic Modulus GPa
0/90°	1250°C/5 h/HCl	165	64.4
0/90°	1250°C/5 h/HCl	168	61.6
0/90°	1200°C/5 h/HCl	152	50.2
+/−45°	1250°C/5 h/HCl	85	45.9
+/−45°	1250°C/5 h/HCl	88	41.9

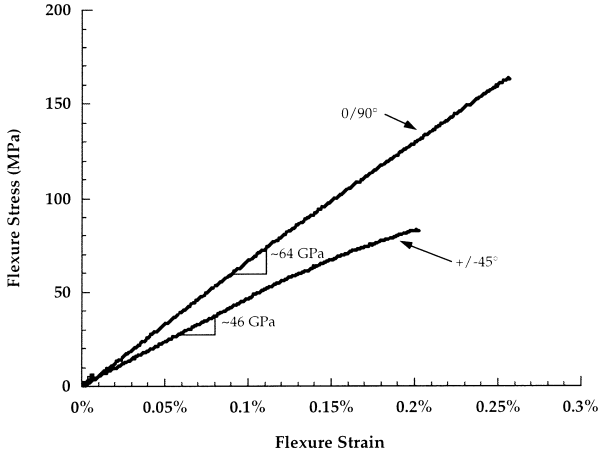

Fig. 6. Flexure stress versus Nominal Flexure Strain plot showing elastic modulus of composite with final sintering at 1250°C for 5 h in HCl. The composite was tested in the in-plane fiber orientation. Tests for fiber weave orientations of 0/90° and +/−45° are shown.

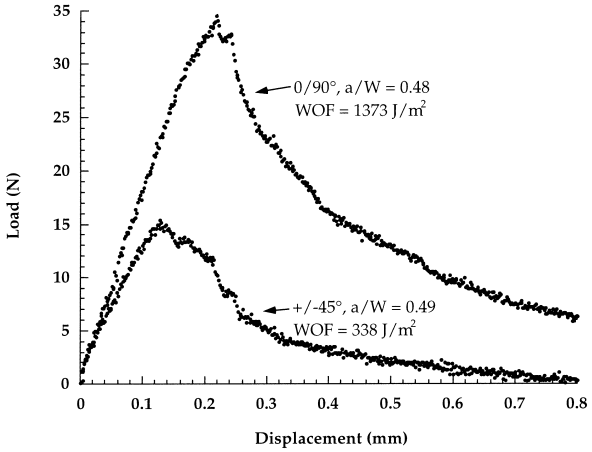

Fig. 7. Load versus displacement plots of notched composite samples tested in the in-plane configuration. Final sintering of composite was at 1250°C for 5 h in HCl. Composite samples with 0/90° and +/−45° fiber orientations are shown. The normalized notch depth for these samples was $a/W = 0.48$ and 0.49, respectively.

Table 2
Properties of in-plane notched composite 3-point bend tests[a]

Fiber	Sintering	WOF J/mm^2	Strength ratio	Net-section stress MPa	K_I at peak load MPa*m$^{1/2}$	K_{ss} MPa*m$^{1/2}$
0/90°	1250°C/5 h/HCl	1373	0.69	115	4.46	9.3
0/90°	1250°C/5 h/HCl	1287	0.66	100	3.89	8.0
+/−45°	1250°C/5 h/HCl	438	0.72	62.4	2.32	4.38
+/−45°	1250°C/5 h/HCl	338	0.62	53.9	2.06	3.85

[a] a/W≈0.49.

3.3. Composite microstructure

Fig. 9 illustrates the fracture region of a 0°/90° specimen. Fig. 9(a) and (b) show that fibers in 0° tows in each cloth layer exhibit random failure to produce 'brushes', or what is known as 'fiber pull-out'. Since no holes are observed in the matrix from where the fibers could have pulled from, it must be concluded that porous matrix between the fibers disintegrated into smaller pieces, and that fibers did not slide out of matrix holes as observed for composites produced with 'weak' interfaces. Some of the matrix debris, and matrix still bonded to the fibers are seen in Fig. 9(c). Fig. 9(d) shows that some fracture regions in the 0° tows have a flatter, more coordinated fracture topography. Close examination of the fibers in this region shows that most of them fracture on different planes, indicating that one crack front did not cause this fracture topography. One can see a few pairs of fibers (arrows) which do exhibit planar fracture; examination of these fiber pairs shows that they have a common fracture origin where they touch. As detailed elsewhere,[21] this common fracture origin was produced during fiber processing. This occurs when adjacent fibers in the bundle (all floors are spun from solution concurrently) stick to each other and sinter together along their cylindrical axis. It was shown that many fiber tows contained pairs of fibers that exhibited this frequent fracture origin.

Fig. 9(a) and (b) shows the planar fracture of the 90° fiber tows in each cloth layer. Here, the crack topography can be characterized as nearly planar, and the surface of this 'planar' region contains relatively long lengths of the 0° fibers extending from the fracture surface [see arrow in Fig. 9(b)]. Fig. 10 shows the fracture surface of the +/−45° oriented specimens. Large areas are seen where the crack path propagated along the cylindrical fiber surfaces (arrows); these cracks jog across fiber tows. The surface produced when the crack propagates across the tow certainly does not form fiber 'brushes', but as shown in the enlarged view, Fig. 10(b), it can be seen that the same crack front did not cause all fibers to fail.

Generally, as shown in Figs. 9 and 10, the ZrO_2 and mullite matrix fills all of the interstices between the fibers. As detailed elsewhere,[6] the HCl treatment at temperatures between 1200 and 1300°C is effective in producing a strong matrix without shrinkage via an evaporation/ condensation sintering and coarsening phenomenon for the ZrO_2 portion of the matrix. The lack of shrinkage of the powder matrix is evident in Figs. 9 and 10 by the lack of crack-like voids in the matrix. If the powder matrix were to densify its shrinkage,

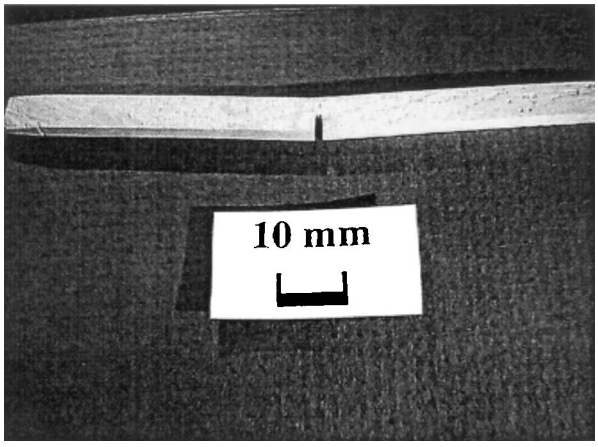

Fig. 8. Photograph of 0/90° composite that was tested with a notch in the in-plane 3-point bending configuration. The sample still holds together due to interlocking fibers even after considerable permanent strain, a/W≈0.5.

constrained by the fibers, would produce regions that are dense and others that are less dense. Eventually, crack-like voids form if it is heated to a high enough temperature.[8,24]

4. Discussion

4.1. Interlaminar shear strength

According to finite element analysis, the shear stresses are much higher than calculated by the classical beam theory equation.[25] They are higher principally at the loading lines and along almost a diagonal line between the upper load point and the lower load points. Close to the top anvil, the maximum shear stress occurs just below the surface (approximately 0.13–0.2 of the normalized sample height).[25] It is suggested that the localized

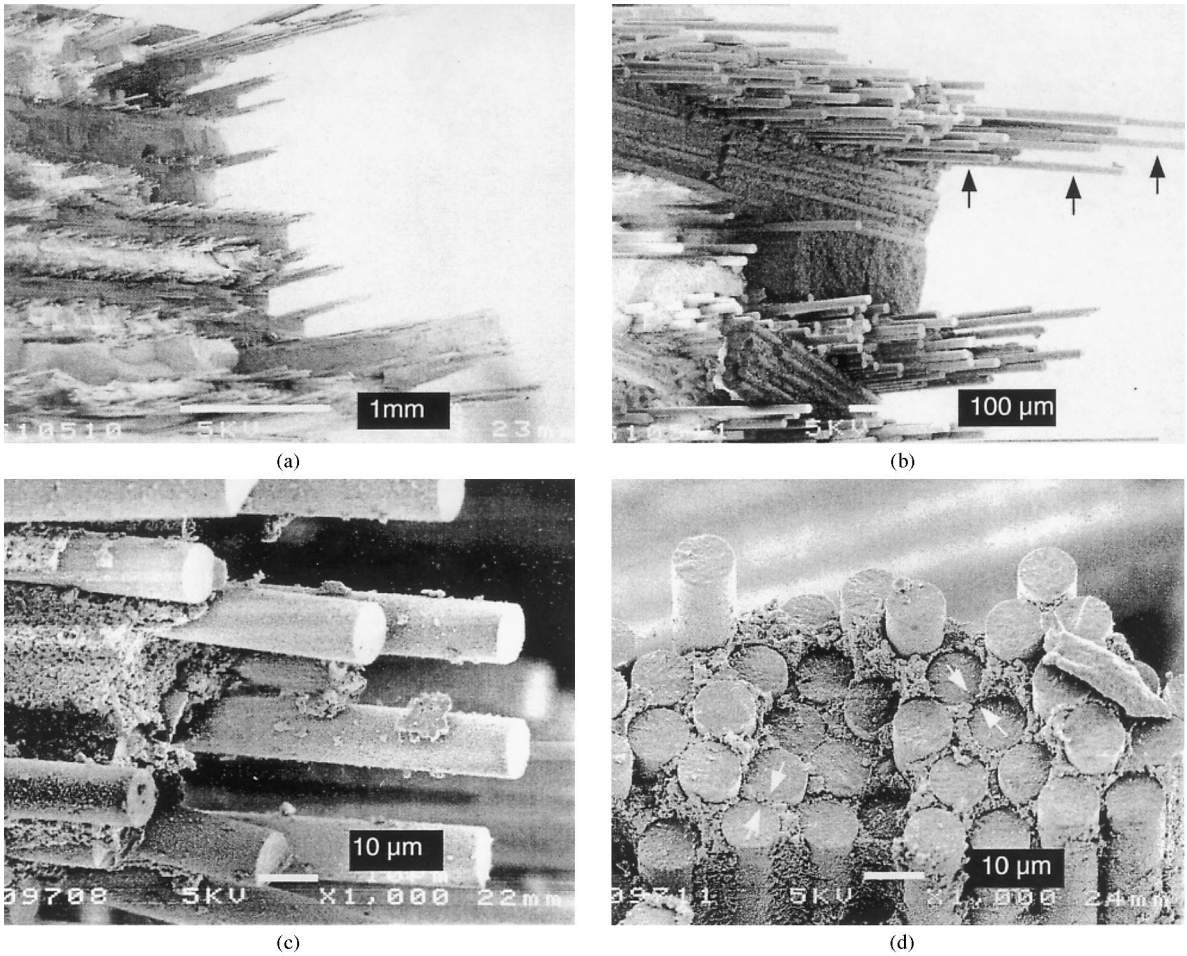

Fig. 9. Fracture surface near the tensile surface of a 0/90° fiber orientation composite containing 70v% cubic ZrO_2 (8m% Y_2O_3)/30v% mullite sintered at 1200°C for 5 h inHCl. The composite was tested in the in-plane 3-point bending configuration. Large amounts of fiber pullout are evident with little coordinated fracture. (a) Low magnification showing general extent of fiber pullout, (b) Higher magnification, arrows show fibers that failed independently and pulled free with disintegration of the surrounding matrix. (c) Micrograph showing fiber pullout and showing portions of the matrix bonded to the fibers indicating a strongly bonded matrix. Matrix between the fiber disintegrated during the fracture process. (d) Micrograph showing a region of fairly coordinated fiber fracture in the 0/90 composite sample although, except for fibers that were bonded together (arrows), the crack plane is unique implying that a continuous crack plane did not exist during fracture even in this region.

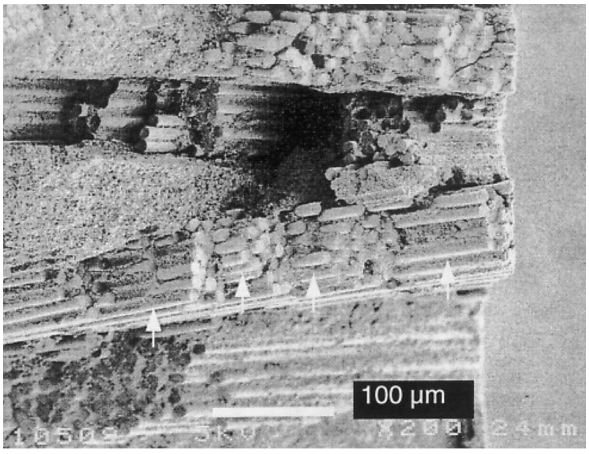

(a)

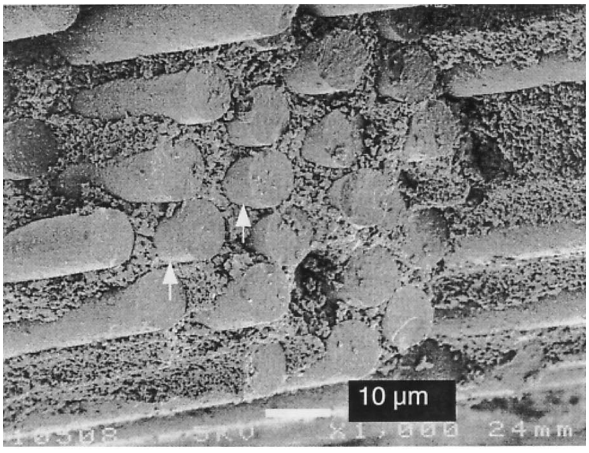

(b)

Fig. 10. Fracture surface near the tensile surface of a +/−45° fiber orientation composite containing 70v% cubic ZrO_2 (8m% Y_2O_3)/30v% mullite sintered at 1250°C for 5 h in HCl. The composite was tested in the in-plane 3-point bending configuration. Very little fiber pullout is evident for in-plane testing in this fiber orientation. (a) Arrows show where the crack propagated along fibers before cutting across part of the tow of fibers. (b) Arrows show that fracture of the fibers was not on a common plane but still independently failed fibers with less disintegration of surrounding matrix.

loading can be reduced by placing compliant materials between the beam and the loading anvil, as attempted here, so that stresses will be distributed more uniformly over a larger area at the loading point.[26] This can be tolerated in this test because it is the shear stress that is of interest rather than the tensile stress on the lower beam.

The short beam bending test that has been used to characterize the interlaminar shear strength of fiber composites is ASTM Standard D2344. However, based on finite element modeling experiments and analytical analysis it is suggested that this type of testing is not accurate for comparing substantially different materials or for design purposes.[25,27,28] This is due to the localized and complicated loading at the loading anvils and due to differences from Euler–Bernouilli beam theory, which requires long beams and assumes pure bending. The general conclusion is that the short beam bend test may be used for comparison of similar materials for interlaminar shear strength.

The results for interlaminar shear strength showed an apparent shear strength dependence of the span to thickness ratio. Work of others has also shown this and concluded that the short beam bend test does not characterize a quantitative interlaminar shear strength.[25,28] This is due to the localized loading conditions at the loading anvils and due to the short beam length. It could be pointed out that the short beam prevents application of St. Venant's principle, which states that stresses become uniformly distributed in a body at a sufficient distance from the loading points. A short beam does not provide sufficient distance to allow the stress distribution to be uniform in the body and so the measured shear strength changes with the span length for a given thickness. Also, as discussed above, the absolute magnitude of the shear strength is uncertain due to the nature of the localized loading.

The 'nominal' interlaminar shear strength for the materials tested varied from 8 to 11 MPa. This is comparable to the alumina and mullite matrix composites made by others.[26] One observation was that lower strengths were measured in specimens that appeared to have more flaws on side edges of the beam. This suggests the possibility that flaws in the matrix microstructure (voids or cracks) may reduce the interlaminar shear strength, but this trend is not clear nor readily quantifiable. In work by others, lower porosity (or higher densities in the matrix) caused increased interlaminar shear strength at the cost of notch insensitivity.[26]

The effort to characterize and improve the interlaminar shear strength of all-oxide composites was due to initial measurements of the properties of the composite in bending to measure a tensile strength. In early tests, not reported here, the composite failed in an interlaminar shear manner. By reducing the thickness of the powder layer between the fiber cloth layers, which is not characterized here, the interlaminar shear strength was improved to that reported in Fig. 3. It appears that with improved processing tensile failure may now limit the performance of the composite for potential applications. Very short spans (or intense localized bending) are needed to produce delamination failure. Further work may determine that 3-D architectures and weaving of layers of the fibers could be effective ways of improving this property of the composite if it is necessary.

4.2. Notch sensitivity and in-plane bend testing

The flexure test provides a measure of the tensile strength of the material. The 0/90° orientation had a flexure strength of about 165 MPa which is comparable to the strengths obtained previously with a porous alumina/

mullite matrix using the 720 fibers.[5] The fact that the composites with the mullite/zirconia matrix have strengths similar to those with a mullite/alumina matrix is a reasonable result if the point of view is taken that the tensile properties in the 0/90° orientation are dominated by the fiber properties. Relative to CMCs with 'weak' interfaces, matrix cracking is not apparent until near the fracture stress, but the porous matrix composites appear to have a somewhat smaller strain to failure. It must be remembered that in most CMCs multiple matrix cracking occurs at a stress much below the fracture stress. Most of these materials have either carbon or BN interphases between the fiber and matrix and contain non-oxide fibers. Multiple matrix cracking would therefore dramatically limit their application in oxidizing conditions. Therefore the allowable design strain could be similar to current CMCs.

The net-section stress at failure in the presence of the notch can be calculated and compared to the strength at failure of an un-notched sample as a measure of notch sensitivity. The net-section strength can be approximated by assuming that all the material above the plane of the notch tip acts to apply load to the remaining un-notch portion of the beam. This can be done by simply subtracting the length of the notch from the height of the beam and using this as the new height. The net-section strength of the notched beams compared to an un-notched beam gives a strength ratio that is an indication of the degree of notch sensitivity of the material. This is shown in Table 2 for the current material. The strength ratio for the notched beams was ≈ 0.7 indicating moderate notch insensitivity. This level of notch sensitivity is greater than that observed with the notched bend test with the mullite/alumina matrix where the ratio is $\sim$0.9.[22]

In addition, the notched beam specimen can be used to determine the work of fracture. Additionally, the work of fracture (WOF) can be related to a steady state toughness (K_{Iss}) of the composite through the simplified equation:

$$K_{Iss} = (\mathrm{WOF}^* E)^{1/2} \quad (5)$$

where E is the elastic modulus of the un-notched sample.

Because there is a crack length over which this fracture toughness develops in composite materials (R-curve behavior), it is important to compare the steady state fracture toughness to the magnitude of the stress intensity caused by the notch at the failure load. The applied stress intensity at the notch tip of a beam in bending can be determined using the following equation:

$$K_I = 2.6^* 6Ma^{1/2}/(b^* t^2), \quad (6)$$

where K_I is the applied stress intensity factor, M is the applied bending moment = Load*Span/4, 'a' is the notch length, 'b' is the beam width, and 't' is the beam thickness. As shown in Table 2, the values of K_I, are about half of K_{Iss} suggesting that the notch lengths in the bend tests are not long enough to reach the steady state toughness of the material. The notch sensitivity of the composite therefore will have a size dependent effect which was not examined here. This crack length effect on the notch sensitivity is similar to that in brittle materials with ductile reinforcements.[29]

4.3. Composite microstructure

In general, the microstructure is consistent with the mechanical properties. In the case of the 0/90° composites, improved toughness is obtained from a microstructure where the fibers can absorb energy of stress concentrations by bridging crack surfaces and dissipating energy as the matrix disintegrates during fiber pull-out as shown in Fig. 9. Fig. 9(c) shows that the particles are bonding to the fibers. This supports the conclusion that the energy absorption during fracture comes from disintegration of the matrix surrounding the fibers. Where these features are absent in the fracture surface lower toughness is observed as in the case of the +/−45° composite samples shown in Fig. 10. However, the 80 MPa strength in the +/−45° floor orientation is higher than the 5O MPa obtained by Levi et al.[5] even for the higher strength 610 fiber. Clearly, the lower fiber strength in the 720 fibers is not reducing the strength for this fiber orientation. The absence of extensive disintegration of the matrix in the +/−45° samples may provide for a higher strength at a cost of a lower strain to failure than is obtained with the 610 fibers. Potentially, a stronger matrix (zirconia/mullite) combined with a lower fiber strength (720 fiber) may be the cause for this result. It should be pointed out, however, that no testing of the mullite/alumina matrix composites with 720 fibers in the +/−45° fiber orientation has been performed. So, a direct comparison is not available. An advantage of the microstructure containing coarsened zirconia and mullite is the coarsening and strengthening without shrinkage. It is also resistant to densification during high temperature, long term use in air. These added benefits make this processing method useful in addition to the benefit of a simplified processing method.

5. Summary

A simple single-step processing method was introduced and evaluated for an all-oxide layered woven fiber composite in this paper. This composite and some of its mechanical properties were also described in this paper. The method uses an infiltration of the all-oxide fibers with sub-micron ceramic particles that results in a

homogenous powder matrix with a very high particle packing density. The use of cubic zirconia particles allows the matrix to be strengthened by a HCl heat treatment that sinters and then coarsens the ZrO_2 portion of the matrix without densification. The coarsening of the ZrO_2 grains makes the matrix resistant to further shrinkage in an air environment. The porous but shrinkage resistant powder matrix provides stability to the matrix that must remain porous to provide the notch insensitivity. The addition of mullite to the matrix further stabilizes the porous microstructure.[6]

Testing of the layered woven fiber composite with the fiber layers horizontal to the bending plane was used to characterize the interlaminar shear strength of the composites. For this composite, there were interlaminar shear failures in the matrix in between the planes of the woven fibers although some anomalies were observed. The interlaminar shear strength was approximately 8–11 MPa. This was in the range of those measured for similar composites using the same woven oxide fibers used here.

Bending tests with the fibers oriented in-plane (vertically) showed that the composite had a strength of 165 MPa, which is comparable to other composites using this type of woven oxide fiber. Moderate notch insensitivity in the 0/90° fiber orientation was shown. The composite produced here appears to have similar properties to other porous oxide matrix composites using this type of fiber but has the advantage of (1) simple processing method and (2) a matrix microstructure that is resistant to densification during use.

Acknowledgements

Research supported under AFOSR award number F49620-96-1-0003. The authors appreciated useful discussions with Dr. Carlos Levi, Dr. James Yang, and Dr. Frank Zolk. Dr. Karl E. Berroth supported on sabbatical leave from Swiss Federal Laboratories for Materials Testing and Research (EMPA).

References

1. Phillips, D. C., Interfacial bonding and the toughness of carbon fiber reinforced glass and glass-ceramics. *J. Mater. Sci.*, 1974, **9**(11), 1847–1854.
2. He, M. Y. and Hutchinson, J. W., Crack deflection at an interface between dissimilar elastic materials. *Int. J. Solids Struct.*, 1989, **25**, 1053.
3. Lange, Fred F., Tu, W. C. and Evans, A. G., Processing of damage-tolerant oxidation-resistant ceramic matrix composites by a precursor infiltration and pyrolysis method. *Mater. Sci. Eng.*, 1995, **A195**, 145–150.
4. Tu, W. C., Lange, Fred F. and Evans, A. G., Concept for a damage-tolerant ceramic composite with strong interfaces. *J. Am. Ceram. Soc.*, 1996, **79**, 417–424.
5. Levi, C. G., Yang, J. Y., Dalgleish, B. J., Zok, F. W. and Evans, A. G., The processing and performance of an all-oxide ceramic composite. *J. Am. Ceram. Soc.*, submitted February 1997.
6. Haslam, J. J. and Lange, F. F., Processing and mechanical Properties of porous mullite and zirconia mixtures sintered by evaporation/condensation sintering, to be published.
7. Zok, F., Lange, F., Porter, F. and John, R., Packing density of composite powder mixtures. *J. Am. Ceram. Soc.*, 1991, **74**(8), 1880–1885.
8. Sudre, O. and Lange, F. F., The effect of inclusions on densification: III, the desintering phenomenon. *J. Am. Ceram. Soc.*, 1992, **75**(12), 3241–3251.
9. Heintz, J.-M., Sudre, O. and Lange, F. F., Instability of polycrystalline bridges that span cracks in powder films densified on a substrate. *J. Am. Ceram. Soc*, 1994, **77**(3), 787–791.
10. Tu, W. C. and Lange, F. F., Liquid precursor infiltration and pyrolysis of powder compacts: II, fracture toughness and strength. *J. Am. Ceram. Soc.*, 1995, **78**(12), 3283–3289.
11. Wilson, D. M., Statistical tensile strength of Nextel 610 and Nextel 720 fibres. *J. Mater. Sci.*, 1997, **32**(10), 2535–2542.
12. Wilson, D. M., Lieder, S. L. and Lueneburg, D. C., Microstructure and high temperature properties of 85% Al_2O_3–15% SiO_2 fibers. *Intermetallic Matrix Composites Ill Symposium*. San Francisco, CA, USA, 4–6, April 1994. ed. J. A. Graves, R. R. Bowman, J. J., Lewandowski, Philadelphia, PA, USA: Mater. Res. Soc, 1994. pp. 89–98.
13. Readey, M. J. and Readey, D. W., Sintering of ZrO_2 in HCl Atmospheres. *J. Am. Ceram. Soc.*, 1986, **69**(7), 580–582.
14. Colic, M., Franks, G., Fisher, M. and Lange, F., Chemisorption of organofunctional silanes or silicon nitride for improved aqueous processing. *J. Am. Ceram. Soc.*, 1998, **81** (9).
15. Klein, S., Fisher, M., Franks. G., Colic, M. and Lange, F., Comparison of the influence on the interparticle pair potentials on the rheological behavior of zirconia: part B — the influence of surfactants, to be published.
16. Chang, J. C., Lange, F. F., Pearson, D. S. and Pollinger, J. P., Pressure sensitivity for particle packing of aqueous Al_2O_3 and ZrO2/Al_2O_3 composite slurries vs interparticle potentials: particle packing and mass segregation. *J. Am. Ceram. Soc.*, 1991, **4**(9), 2201–2204.
17. Franks, G. V., Colic, M., Fisher, M. L. and Lange, F. F., Plastic-to-brittle transition of consolidated bodies: effect of counterion size. *J. Colloid Interface Sci.*, 1997, **193**, 96–103.
18. Franks, G. V., Velamakanni, B. V. and Lange, F. F., Vibraforming and in-situ flocculation of consolidate, coagulated alumina slurries, *J. Am. Ceram. Soc.* **78** (5), 1324,1328 (1995). and US Patent 5, 188, 780, Method for preparation of dense ceramic products, B.V. Velamakanni, and F.F. Lange, Feb.23, 1993.
19. Lange, F. F., Effect of interparticle potentials on particle packing for ceramic processing, *Powders and Grains 93*. A. A. Balkema Press, Rotterdam, 1993.
20. Berroth, K. E., Haslam. J. J. and Lange, F. F., Swiss Patent number 1998 1317/98. Process for the fabrication of ceramic fiber composite material and components. Also US Patent pending.
21. Haslam, J. J. and Lange, F. F., Observations on the effects of heat treatments in HCl on the fiber bundle strength of a two-phase polycrystalline oxide fiber, to be published.
22. Heathcote, J. A., Gong, X.-Y., Yang, J., Ramamurty, U. and Zok, F. W., In-plane mechanical properties of an all-oxide ceramic composite, submitted to *J. Am. Ceram. Soc.*, April, 1998.
23. Folsom, C. A., Zok, F. W. and Lange, F. F., Mechanical behavior of a laminar ceramic/fiber-reinforced epoxy composite. *J. Am, Ceram. Soc.*, 1992, **75**(11), 2969–2975.
24. Lam, D. C. C. and Lange, F. F., Microstructural observations on constrained densification of alumina powder containing a periodic array of sapphire fibers. *J. Am. Ceram. Soc.*, 1994, **77**(7), 1976–1978.
25. Berg, C. A., Tirosh, J. and Israeli, W., Analysis of short beam bending of fiber reinforced composites. In *Composite Materials:*

Testing and Design (Second Conference), ASTM STP 497, American Society for Testing and Materials, 1972, pp. 206–218.
26. Mattoni, M. and Zok, F., unpublished work.
27. Whitney, J. M. and Browning, C. E., On short-beam shear tests for composite materials. *Experimental Mechanics*, September 1985, pp. 294–300.
28. Xie, M. and Adams, D. F., Study of three- and four-point shear testing of unidirectional composite materials. *Composites*, 1995, **26**, 653–659.
29. Bao, G. and Zok, F., On the strength of ductile particle reinforced brittle matrix composites. *Acta Metall. Mater*., 1993, **41**(12), 3515–3524.